J Proteomics. Author manuscript; available in PMC 2013 July 11.

Published in final edited form as:
J Proteomics. 2009 August 20; 72(6): 960–973. doi:10.1016/j.jprot.2009.04.003.

Proteomic analysis of enriched lysosomes at early phase of camptothecin-induced apoptosis in human U-937 cells

Nicolas Parent[a], **Eric Winstall**[b], **Myriam Beauchemin**[a], **Claudie Paquet**[a], **Guy G. Poirier**[b], and **Richard Bertrand**[a,c,*]

[a]Centre de recherche, Centre hospitalier de l'Université of Montréal (CHUM), Hôpital Notre-Dame and Institut du cancer de Montréal, Montréal (QC), Canada H2L 4M1

[b]Centre de recherche, Centre hospitalier de l'Université Laval (CHUL), Québec (QC), Canada G1V 4G2

[c]Département de médecine, Université de Montréal, Montréal (QC), Canada H3C 3J7

Abstract

A lysosomal pathway, characterized by partial rupture or labilization of lysosomal membranes and cathepsin activation, is evoked during camptothecin-induced apoptosis in human cancer cells, including human histiocytic lymphoma U-937 cells. These lysosomal events begin rapidly and simultaneously with mitochondrial permeabilization and caspase activation within 3 h after drug treatment. In this study, comparative and quantitative proteome analyses were performed to identify early changes in lysosomal protein expression/localization from U-937 cells undergoing apoptosis. In 2 independent experiments, among a total of more than 538 proteins putatively identified and quantitated by iTRAQ isobaric labeling and LC-ESI-MS/MS, 18 proteins were found to be upregulated and 9 downregulated in lysosomes purified from early apoptotic compared to control cells. Protein expression was validated by Western blotting on enriched lysosome fractions, and protein localization confirmed by fluorescence confocal microscopy of representative protein candidates, whose functions are associated with lysosomal membrane fluidity and dynamics. These include sterol-4-alpha-carboxylate 3-dehydrogenase (NSDHL), prosaposin (PSAP) and protein kinase C delta (PKC-δ). This comparative proteome analysis provides the basis for novel hypothesis and rationale functional experimentation, where the 3 validated candidate proteins are associated with lysosomal membrane fluidity and dynamics, particularly cholesterol, sphingolipid and glycosphingolipid metabolism.

Keywords

Apoptosis; Camptothecin; Lysosome; iTRAQ reagent; LC-ESI-MS/MS; Confocal Microscopy

*Corresponding author. CRCHUM, Hôpital Notre-Dame and Institut du cancer de Montréal, 1560 Sherbrooke St. East (Room Y-5634), Montreal (QC), Canada H2L 4M1. Tel.: +1 514 890 8000x26615; fax: +1 514 412 7591. richard.bertrand@umontreal.ca (R. Bertrand).

1. Introduction

The lysosomal pathway of apoptosis involves moderate rupture of lysosomes, often referred to as small-scale lysosomal rupture or lysosomal labilization, and subsequent release of lysosomal cathepsins into the cytosol [1–4]. Lysosomal rupture and cathepsin activation have been linked to apoptosis after various insults, including oxidative stress [5], lysosomotropic photo sensitizer agents [6,7], serum withdrawal [5], Fas and tumor necrosis factor-alpha (TNF-α) ligation [5,8], increased sphingosine [9] and endogenous ceramide levels [10], DNA-damaging [11,12] and microtubule-stabilizing agents [13]. During 20-S-camptothecin (CPT)-induced apoptosis in U-937 and Namalwa cancer cells, lysosomal labilization and cathepsin B activation occur rapidly and simultaneously with mitochondrial permeabilization and caspase activation, effects prevented by Bcl-xL, indicating that lysosomal rupture may be related, in part, to mitochondrial disruption [12].

Alterations of mitochondrial functions, such as mitochondrial permeability transition, transmembrane potential disruption, ATP/ADP exchange and cytochrome c release, are early events involved in the initiation step of apoptosis induced by most chemotherapeutic agents [14–20]. Members of the Bcl-2 family of proteins are critical regulators of the mitochondrial pathway of apoptosis that either promote cell survival (e.g. Bcl-2, Bcl-xL, Bcl-w, Mcl-1) or facilitate cell death. The pro-cell death members are subdivided into 2 classes: multidomain proteins that contain Bcl-2 homology (BH) domains 1–3 (e.g. Bax, Bak), and BH3-only proteins constituted of a unique BH3 motif (e.g. Bad, Bid, Bik, Bim, Puma, Noxa, Hkr) [21,22]. Relative amounts and localization of death agonists and antagonists greatly influence the cell's ability to undergo apoptosis. Because it provides binding ability, the BH3 motif has become a potent mediator of cell death and is often uniquely required for cell-killing activity [23,24]. Two distinct models have been proposed to explain the killing activity of BH3-only proteins [22]. The *direct activation model* proposes that after a death stimulus, BH3-only proteins promote apoptosis by binding to and inhibiting pro-survival Bcl-2 family members, or by binding to other death agonists, like multidomain Bax and Bak proteins, which become activated and exert their pro-apoptotic activities at the mitochondrial level. BH3-only proteins that neutralize pro-survival proteins are referred to as BH3 "enabler or sensitizing" proteins, while those that bind pro-apoptotic Bax or Bak are called BH3 "activator or activating" proteins [25–27]. The *indirect activation model* suggests that all BH3-only proteins solely engage pro-survival proteins and act by preventing them from inhibiting Bax or Bak activation [28–30].

In contrast, the exact mechanisms that influence lysosomal membrane stability during apoptosis induced by DNA-damaging agents are, yet, not resolved. The best-studied models have associated lysosomal membrane rupture with oxidative stress, accumulation of redox-active iron and the occurrence of a lipid peroxidative chain reaction (for review see [4]). It has also been reported that sphingosine, a metabolite of the sphingomyelin and ceramide pathway, and lysophosphatidylcholine, a phospholipase A2-produced lipid metabolite, are capable of eliciting relatively selective damage to the lysosomal membrane, provoking lysosomal rupture [9,31]. Although the exact mechanisms behind the relative activity of sphingosine and lysophosphatidylcholine for lysosome destabilization have not been fully clarified, it has been proposed that sphingosine is a lysosomotropic detergent because its

long hydrophobic tail and polar head contain a proton-trapping group that is attracted by the acidic lysosomal vacuolar compartment [9], while lysophosphatidylcholine changes lysosomal osmotic sensitivity provoking entry of potassium ions leading to losses of membrane and lysosomal integrity [31]. Only a few proteins have been associated with lysosome labilization during apoptosis. First, cytosolic phospholipase A2 was proposed to attack the lysosomal membrane, provoking its destabilization [32]. Other studies have suggested that phospholipase A2 and C could osmotically destabilize the lysosome membrane via a K(+)/H(+) exchange process [33–36], effects associated with lysophosphatidylcholine [31]. More recently, the accumulation of lysosome-associated apoptosis-inducing protein containing pleckstrin homology and FYVE domains (LAPF) on lysosomal membranes was also linked with lysosomal rupture and activation of a lysosomal-mitochondrial pathway of apoptosis [37].

In this study, to identify proteins putatively associated with lysosome labilization in the early phase of apoptosis induced by DNA-damaging agents, comparative and quantitative proteomic analyses of enriched lysosomes were performed in CPT-induced apoptosis of human histiocytic lymphoma U-937 cells. A significant proportion of the proteins putatively quantitated and identified by iTRAQ reagent labeling and LC-ESI-MS/MS play a role in membrane dynamics and fluidity, vesicle trafficking, redox regulation, cellular stress response and signaling pathways. In 2 independent experiments, 2 proteins were reproducibly found to be upregulated (>1.5) and 2 downregulated (<0.75) in lysosomes purified from early apoptotic compared to control cells. Considering the dynamic nature of small membrane-bound organelles and the restrictive and limiting criteria of the study consisting of experiments performed at very early phase of apoptosis when approximately less than 10% of the lysosome population presents partial membrane disruption or labilization, 16 candidate proteins found to be upregulated, and 7 downregulated, in 1 experiment only, were also considered. Finally, a rationale approach for validation of representative candidate protein was taken, based on the fundamental biological question addressed in this study, which is related to biomembrane fluidity and dynamics.

2. Materials and methods

2.1. Cell line, chemicals and drug treatment

Human histiocytic lymphoma U-937 cells obtained from the American Type Culture Collection (Manassas, VA), were grown in suspension at 37 °C under 5% CO_2 in RPMI-1640 medium supplemented with 10% heat-inactivated fetal bovine serum, 2 mM glutamine, 100 U/ml penicillin and 100 μg/ml streptomycin (Gibco-BRL Life Technologies, Grand Island, NY). CPT, Histodenz™, Hoechst 33342 and propidium iodide (PI) were obtained from the Sigma-Aldrich Company (St. Louis, MO). Percoll™ was purchased from GE Healthcare Bio-Sciences AB (Uppsala, Sweden). Acridine orange (AO), 5,5′,6,6′-tetrachloro-1,1′,3,3′-tetraethylbenzimidazolyl-carbocyanideiodide (JC-1), LysoTracker RED/DND-99, MitoTracker Green/FM and ER-Tracker Red dye were purchased from Molecular Probes (Eugene, OR). The fluorogenic peptide derivatives acetyl-Asp-Glu-Val-Asp-7-amino-4-methylcoumarin (Ac-DEVD-AMC) and benzyloxycarbonyl-Arg-Arg-7-amino-4-methylcoumarin (Z-RR-AMC) were acquired from Calbiochem–Novobiochem

Corporation (San Diego, CA). All other chemicals were of reagent grade and purchased either from the Sigma-Aldrich Company, ICN BioMedicals (Costa Mesa, CA) or other local sources. For drug treatment, U-937 cells were treated with CPT at a concentration of 1.0 μM for 30 min, and then grown in drug-free medium.

2.2. Loss of mitochondrial transmembrane potential (↓ΔΨm) and lysosomal rupture

↓ΔΨm was assessed by JC-1 staining [12,38]. At the indicated times (h) after CPT treatment, 1×10^6 cells were incubated with 10 μg/ml JC-1 in complete culture medium for 15 min at room temperature, washed twice, resuspended in 500 μl of PBS and submitted to flow cytometry analysis. To assess lysosomal rupture, at various times after drug treatment, 1×10^6 cells were incubated with 1 μM AO in complete culture medium for 15 min at 37 °C; then, the cells were washed twice and resuspended in 500 μl of fresh culture medium before analysis by flow cytometry (uptake method) [5,12]. Loss of JC-1 orange fluorescence was measured with the FL2 channel, loss of lysosomal AO red fluorescence with the FL3 channel, and increased cytosolic AO green fluorescence with the FL1 channel of a Coulter EPICS XL-MLC Flow Cytometer. At least 10,000 cells per sample were acquired in histograms, and the results are expressed as the percentage of total cells presenting ↓ΔΨm or lysosomal rupture.

2.3. Analysis of DNA fragmentation

The kinetics of DNA fragmentation were monitored and quantitated by DNA filter elution assays, and the results expressed as percentages of DNA fragmentation [39]. DNA content was also measured by flow cytometry after PI staining with recording on the FL2 channel of the Coulter EPICS XL-MLC Flow Cytometer. The results are expressed as percentages of cells presenting hypoploid DNA content (sub-G1 peak).

2.4. Enzymatic assays

For the measurement of enzyme activities, cellular extracts were prepared in lysis buffer containing 100 mM Hepes (pH 7.5), 5 mM EDTA, 5 mM DTT, 20% (v/v) glycerol and 0.3% (v/v) Igepal. Protein aliquots (100 μg) were incubated with 200 μM of the caspase-3-like substrate Ac-DEVD-AMC or with 20 μM of the cathepsin B substrate Z-RR-AMC, in reaction assay mixtures (500 μl) containing 100 mM Hepes (pH 7.5), 100 mM NaCl, 10% glycerol, 0.1% (w/v) CHAPS, 10 mM DTT and 1 mM EDTA for caspase-3-like activity, and 0.4 mM sodium acetate buffer (pH 5.5) and 4 mM EDTA for cathepsin B activity. Enzymatic activities were determined as initial velocities at 37 °C in a dual luminescence fluorometer at an excitation wavelength of 380 nm and an emission wavelength of 460 nm, and expressed as relative intensity/min/mg.

2.5. Subcellular fractionation

A 2-step sequential density gradient centrifugation protocol was modified from Storrie and Madden [40] and Paquet et al. [41] for lysosome isolation. A schematic representation of the procedure is illustrated in Supplemental Fig. 1. First, control and CPT-treated U-937 cells (5.0×10^8) were swelled in deionized water for 4 min on ice, and the samples adjusted to 220 mM mannitol, 70 mM sucrose, 10 mM Hepes-KOH (pH 7.4) and 1.0 mM EDTA (isotonic

buffer). The cells were then disrupted by passing the samples 30-fold through a 26G3/8 needle, and subsequently centrifuged at 1000 ×*g* for 15 min to pellet unbroken cells and nuclei. Supernatants containing mitochondria, lysosomes and other vesicles were adjusted to 8 mM calcium chloride and centrifuged at 5000 *g* for 15 min to pellet the rough endoplasmic reticulum and mitochondria. Then, the supernatants were layered on top of the first gradient consisting, from bottom to top, of 2 ml of 35% (w/v) Histodenz™, 2 ml of 17% (w/v) Histodenz™, and 5 ml of 6% (v/v) Percoll™ in isotonic buffer. After centrifugation at 50,500 ×*g* for 1 h at 4 °C, a set of 2 discrete bands appears at the interfaces of 17/35% Histodenz™ and 6% Percoll™/17% Histodenz™. The upper band, at the 6% Percoll™/17% Histodenz™ interface, contained small mitochondria and lysosomes that needed further separation by the second gradient to obtain pure organelle fractions. This interface was collected and adjusted to 35% Histodenz™ by mixing with a 80% (w/v) Histodenz™ solution. The sample was then placed at the bottom of the second gradient and overlaid with 2 ml of 17% Histodenz™ and 5 ml of 5% Histodenz™. The tube was filled to the top with isotonic buffer, and centrifuged at 50,500 ×*g* for 1 h at 4 °C. Two distinct bands appeared: the upper one at the 5/17% Histodenz™ interface contains lysosomes, while the lower one, at the 17/35% Histodenz™ interface, contained small mitochondria. To pellet the lysosomes, the interface was diluted with the largest possible volume of isotonic buffer and centrifuged at 53,000 ×*g* for 1 h at 4 °C.

2.6. Protein digestion and iTRAQ labeling

Relative quantification experiments were performed in duplicate in distinct lysosome preparations. Protein aliquots of lysosomes isolated from normal or apoptotic cells were acetone-precipitated. Each protein pellet was then solubilized in 0.5 M triethylammonium bicarbonate, pH 8.5, supplemented with 0.1% (w/v) SDS. Twenty-five and 80 μg of proteins were used for iTRAQ labeling in the first and second experiment, respectively. Protein cysteine residues were reduced with 5 mM Tris (2-Carboxyethyl) phosphine for 1 h at 60 °C and then blocked with 8 mM methyl methane-thiosulfonate (MMTS) for 10 min at room temperature. Protein samples were digested with 5 μg of modified porcine trypsin in the presence of 10 mM $CaCl_2$ for 18 h at 37 °C. The final SDS concentration at this point was 0.05% (w/v). The efficiency of protein digestion was assessed by SDS-polyacrylamide gel electrophoresis in undigested and digested aliquots of proteins. In both experiments, tryptic peptides from normal cell lysosomes and apoptotic cell lysosomes were labeled with iTRAQ 114 and iTRAQ 117 reagents, respectively, according to the manufacturer's protocol (Applied Biosystems, Foster City, CA). Labeled samples were then combined and dried in a vacuum concentrator.

2.7. Isoelectric focusing of iTRAQ-labeled peptides

Lyophilized iTRAQ-labeled peptides were resuspended in 325 μL of Milli-Q water containing 0.25% (v/v) ampholyte (Bio-Lyte 3/10 Ampholyte, Bio-Rad, Hercules, CA). The resulting solution served to rehydrate an 18-cm IPG gel strip (pH 5–8) from Bio-Rad, for 10 h. Conditions for isoelectric focusing of peptides were as follows: 250 V for 15 min, 10,000 V for 3 h, 10,000 V for 60,000 V h and then at 50 V until the peptides were extracted. Excess overlaying oil was gently blotted away from the IPG strip, which was cut into 36 pieces of 5 mm each. The IPG strip pieces were transferred to a 96-well plate, and peptides

were eluted from the gel pieces by 2 successive extractions (15 min each with shaking) that were subsequently pooled. The first extraction was in 100 μL of a 1% formic acid, 2% acetonitrile solution, and the second extraction was in 100 μL of a 1% formic acid, 50% acetonitrile solution. The extracted peptides were then dried in a vacuum concentrator and resuspended in 25 μL of a 0.1% formic acid solution.

2.8. MS of iTRAQ-labeled peptides

For each analysis, 5 μL of the peptide solution was injected into the nano LC-ESI-MS/MS system. MS analyses were performed in a QStar XL Hybrid ESI quadrupole time of flight tandem mass spectrometer (Applied Biosystems/MDS Sciex) interfaced with an integrated online capillary LC system consisting of an autosampler, switching pump, and micro-pump (LC Packings, Sunnyvale CA). Peptides were first trapped and concentrated on a 300-μm i.d.×5-mm C18 reverse-phase pre-column (LC Packings) at a flow rate of 15 μL/min. The peptide mixture was then separated on a 75-μm i.d.×10-cm BioBasic (New Objective Inc., Woburn, MA) C18 reverse-phase capillary column at a flow rate of 200 nL/min. The gradient started at 98% buffer A (0.1% formic acid in water) and 2% buffer B (0.1% formic acid in acetonitrile) for 5 min, followed by an increase from 2% to 25% in buffer B over 85 min, then from 25% to 40% buffer B over 10 min, and 40% to 80% buffer B over 5 min. The column was washed with 80% buffer B for 5 min and equilibrated at 2% buffer B for 20 min. Eluted peptides were electrosprayed through a distal-coated silica tip (15 μm i.d.) (New Objective Inc.) with an ion spray voltage of 2800 V. Data acquisition on the mass spectrometer was in the positive ion mode within a mass range of 400–1600 m/z for precursor ions for a 1-s period. Information-dependent acquisition of the MS/MS data was performed on the 3 most abundant peptides exceeding 15 counts with +2 to +4 charge states within a 100 to 2000 m/z value window. Time summation of the MS/MS events was set to 3 s. Fragmented target ions were dynamically excluded for 60 s with 100 ppm mass tolerance.

2.9. Data analysis

For iTRAQ, raw data file (.wiff) processing, protein identification, protein quantification, and statistical analyses were undertaken with ProteinPilot v.2.0 software (Applied Biosystems, MDS-Sciex) running the Paragon algorithm [42]. Searches were conducted against a subset of the UniRef100 protein database (version 12.7) containing only entries from Homo sapiens (83 425 protein sequences). The search parameters allowed a peptide and fragment mass deviation of up to 0.2 Da and 1 missed trypsin cleavage. Cysteine modification by MMTS, oxidation of methionine as well as iTRAQ labeling of N-termini of the peptides and side chains of lysine and tyrosine residues were allowed. Peak areas for each of the 2 reporter ions (m/z: 114 and 117) were corrected to account for isotopic overlap according to the manufacturer's instructions. Protein identification and quantification results were calculated and viewed with Protein-Pilot v.2.0. Protein iTRAQ ratios were corrected for experimental bias by the median average protein ratio as correction factor. Only peptides above 80% confidence were used for identification and quantification, and only proteins, including at least 2 peptides above 80% confidence, were considered. The quantification results were reviewed manually for all proteins found to be differentially expressed (iTRAQ ratio >1.5 or <0.75) and for those included in Table 1 and in Supplemental Tables 1 and 2. Briefly, this validation step included the examination of the MS/MS spectrum assigned to

each identified peptide looking specifically for: 1) the presence of the iTRAQ reporter peaks, 2) a good representation of both x and y ions with preferences toward the presence of more than 3 consecutive assigned ions, 3) the assignment of all major peaks of the spectrum, and 4) the signal-to-noise ratio of peaks assigned to peptide fragment ions. Assigned spectra that failed to pass these requirements were not included in the calculation of the protein iTRAQ ratio and not considered for protein identification. Quantification data from very low intensity spectra were removed from the protein ratio calculation. Doubtful identifications were rejected. iTRAQ ratios presented in Table 1 and Supplementary Table 1 represent protein ratios calculated by ProteinPilot v.2.0 based on the weighted average Log ratios of peptides. The significance of the changes in protein expression is reported in Table 1 and Supplementary Table 1 as a *p*-value calculated by the ProteinPi-lot software v 2.0 and reporting the probability that the observed ratio is different from 1 by chance. The accuracy of iTRAQ protein ratios can be assessed from the error factors (EF) values calculated by the ProteinPilot software v.2.0 and reported in Table 1 and Supplementary Table 1. The true value for the average protein ratio is expected to be found between [(reported ratio)* (EF)] and [(reported ratio)÷(EF)], 95% of the time. Standard deviation (S.D.) was calculated by MicrosoftExcel software v.11.2.3. Functional classification of proteins identified in this study was based on information from UniPro Knowledgebase and from published literature in Medline.

2.10. Immunoblotting

For immunoblot experiments, pellets of purified lysosomes were lysed in buffer containing 50 mM Tris (pH 7.4), 120 mM NaCl, 1% Triton X-100, 1 mM sodium orthovanadate, 2 mM phenylmethylsulfonyl fluoride, 5 mM sodium pyrophosphate and a cocktail of protease inhibitors (Complete™, Roche Molecular Biochemicals, Laval, QC, Canada) at 4 °C for 30 min, centrifuged, and the supernatants analyzed by immunoblotting. The primary antibodies in this study were: anti-LAMP-1 mouse mAb LY1C6, EMD BioSciences, Inc (La Jolla, CA); anti-LAMP-1 rabbit pAb H-228, Santa Cruz Biotechnology, Inc. (Santa Cruz, CA), anti-porin 31HL (VDAC-1) mouse mAb 89-173/025, EMD BioSciences, Inc.; anti-Calnexin rabbit pAb sc-11397, Santa Cruz Biotechnology, Inc.; anti-NSDHL (sterol-4-alpha-carboxylate 3-dehydrogenase) rabbit pAb HPA000248, Atlas Antibodies AB (Stockholm, Sweden); anti-protein kinase C-delta (PKC-δ) pAb 658-676, EMD BioSciences, Inc.; anti-prosaposin (PSAP) mouse mAb 1D1-C12, Abnova Corp.; and anti-ERp19 rabbit pAb 10291, Abcam Inc. The secondary antibodies were horseradish peroxidase-conjugated sheep anti-mouse immunoglobulin (Ig) and horseradish peroxidase-conjugated donkey anti-rabbit Ig secondary antibodies (GE Healthcare Bio-Sciences AB). ECL reagents also were from GE Healthcare Bio-Sciences AB. Relative densitometry analysis of Westerns blots are based on integrated *Volume* value (intensity x mm^2) normalized to corresponding loading control (LAMP-1) *Volume* value, performed with Quantity One software (BioRad, Hercules, CA.). The data are expressed as relative ratios (control:CPT-treated) and represent the means of n independent experiments in distinct lysosome preparations.

2.11. Immunofluorescence microscopy

For enriched lysosome staining *in vitro*, aliquots of the preparations were labeled for 20 min in the presence of LysoTracker RED/DND-99 (10 μg/ml), MitoTracker Green/FM (10 μg/

ml), ER-Tracker Red dye (10 μg/ml) or Hoechst 33342 (10 μg/ml) in isotonic buffer, washed twice and spread on glass slides. Images were generated with a Nikon Optiphot-2 microscope equipped with Omega Optical Emission/Excitation Filter Sets XF-21, XF102-2 and XF05-2 and mounted with a thermoelectrically-cooled CCD camera (Model DC330E, DageMTI Inc., Michigan City, IN) hooked up to a PC computer. For co-localization experiments, control and CPT-treated U-937 cells were spread by cytocentrifugation on glass slides and fixed in ice-cold methanol:acetone for 2–3 min. Nonspecific binding sites were blocked with 5% BSA in the presence of irrelevant antibodies (anti-sheep IgG, 10 μg/ml; Sigma-Aldrich) then, the slides were incubated sequentially with the first antibody (candidate proteins) at 10 μg/ml, followed by a fluorescein-conjugated secondary Ab (InVitrogen Molecular Probe; 1:25 v/v), then LysoTracker Red DND-99 or ER-Tracker Red dye or anti-LAMP1 staining at 10 μg/ml and a Texas-red linked secondary Ab (GE Healthcare Bio-Sciences AB; 1:25 v/v). Each antibody incubation for 60 min was followed by several washes in phosphate-buffered solution. Total cells were stained with hematoxylin, and nuclei, with the DNA intercalator Hoechst 33342. The slides were mounted with polyvinyl alcohol 4-88 mounting medium (Sigma-Aldrich). Images were generated and analyzed with a Leica TC S SP5 Confocal Microscope mounted with 3 lasers, Argon, SS561 and HeNe, and equipped for spectral imaging and analysis. *Relative colocalization area* (RCA) values were calculated according to the formula: $[(\mu m2)\text{-}^{YELLOW}/(\mu m2)^{RED}+(\mu m2)^{GREEN}+(\mu m2)^{YELLOW}]\times 100$, where each color was assigned to a defined color spectrum by Clemex Vision software (Version 3.0.036, Clemex, Longueuil, QC, Canada).

3. Results

3.1. Lysosomes are disrupted after CPT treatment in U-937 cells

Human histiocytic lymphoma U-937 cells are highly sensitive to DNA damage and rapidly die by apoptosis after short, 30-min treatment with the DNA-damaging drug CPT, a DNA topoisomerase I inhibitor [12,43,44]. The apoptotic death of these cells is associated with quick involvement of a mitochondrial and lysosomal pathway, within 2–3 h after drug treatment. ↓ΔΨm (Fig. 1a), lysosome membrane labilization (Fig. 1b), activation of caspase-3-like and cathepsin B enzymes (Fig. 1c), DNA fragmentation and sub-G1 cell populations (Fig. 1d) rapidly appear in CPT-treated U-937 cells [12]. Alterations of mitochondrial functions and mitochondrial membrane permeabilization have been studied extensively in the past. For a better understanding of the molecular mechanisms provoking lysosomal rupture, highly-enriched lysosomes were obtained from control and CPT-treated U-937 cells by 2-step sequential density gradient centrifugation, 3 h after treatment. A schematic view of the purification procedure appears in Supplemental Fig. 1. The purity of these lysosome preparations was established first by *in vitro* staining with the fluorescent biomarkers LysoTracker RED/DND-99 (lysosome), MitoTracker Green/FM (mitochondria), ER-Tracker Red dye (endoplasmic reticulum, ER) and Hoechst 33342 (nucleus), observed under a fluorescent microscope (Fig. 2a). In parallel, the purified preparations were incubated and labeled with specific antibodies directed against the protein biomarker LAMP-1 (lysosome), VDAC-1 (mitochondria), Calnexin (ER) and Nucleolin (nucleus) and monitored by fluorescence microscopy (Fig. 2b). The micrographs show much stronger staining with LysoTracker RED/DND-99 (Fig. 2a) and LAMP-1 (Fig. 2b), revealing high

enrichment of the preparations. Similarly, detection of the protein biomarkers by Western blotting (Fig. 2c) indicates similar high enrichment of the lysosome preparations, with high LAMP-1 expression. Finally, fluorescence confocal microscopy experiments were performed to validate LAMP-1 colocalization with the fluorescent biomarker LysoTracker RED/DND-99 (Fig. 2d). The micrographs reveal strong colocalization between LAMP-1 and LysoTracker RED/DND 99 with a *RCA* value of 39.0%±2.7 (n=3), while VDAC-1:LAMP-1 (*RCA*: 11.3%±1.2; n=3), Calnexin:LAMP-1 (*RCA*: 2.3%±0.2; n=3) and Nucleolin:LAMP-1 (*RCA*: 1.9%±0.9; n=3) do not significantly colocalize together (Fig. 2d).

3.2. Differentially expressed proteins identified by MS of iTRAQ-labeled peptides

Proteins of enriched lysosomes obtained from control and at early phase of CPT-treated U-937 cells (3 h post-treatment) were trypsin-digested, labeled with iTRAQ114 and iTRAQ117 reagents, respectively, combined and fractionated by 1-D/IEF. The isoelectric focusing strips were cut into 36 pieces and the peptides eluted. Nano-LC separation, ionization, quantitation and identification of the peptides were performed by the nano-LC-ESI-MS/MS system. A functional classification of proteins identified in this study (reference experiment) is presented in Fig. 3, with data in Supplementary Table 1. Only proteins including at least 2 peptides above 80% confidence, were considered. A significant proportion of all proteins identified in this study has been identified by others, including 55 of the 103 proteins (53.3%) analysed by Hu Z.-Z. et al. [45] and 94 of the 222 proteins (42.3%) reported by Casey T.M. et al. [46], although the lysosome purification in these studies were carried on different tissues or cell types. In the 2 independent experiments on distinct lysosome preparations, 2 proteins were reproducibly found to be upregulated with a mean fold change (FC) >1.50 and 2 were downregulated with mean FC<0.75 in lysosomes purified from apoptotic compared to control cells (Table 1; Level 1). To gain more valuable information of the analysis, and considering the dynamic nature of membrane-bound small vesicules, particularly in a biological context of early phase apoptosis where less than 10% of the lysosome population presents partial membrane disruption or labilization, candidate proteins identified as differentially expressed in 1 experiment only were also considered, and included an additional 16 proteins upregulated and 7 downregulated (Table 1; Level 2 and 3). Peptide listing with identification and quantitation data of the candidate proteins are presented in Supplemental Table 2 with the annotated-spectra for unique-peptide-based protein identification provided in Supplemental Table 3.

3.3. Expression and localization validation by Western blotting and fluorescence confocal microscopy

Considering the fundamental biological question behind this study, which is to understand lysosomal membrane disruption at early phase of apoptosis, a rationale approach for validation of representative candidate protein was taken, based on their function associated with biomembrane fluidity and dynamics. Western blotting analysis was first performed on candidate proteins, including sterol-4-alpha-carboxylate3-dehydrogenase (NSDHL) (Fig. 4a, upper panel), prosaposin (PSAP) (Fig. 4b, upper panel) and protein kinase C delta (PKC-δ) (Fig. 4c, upper panel). Expression levels of NSDHL, PSAP and PKC-δ appeared to be higher at very early phase of apoptosis activation in lysosome preparations obtained from CPT-treated cells (3 h post-treatment) compared to control cells, with relative ratios

(control:CPT-treated; 50 μg protein per lane) of 1:1.30±0.12 (NSDHL; *n*=3), 1:1.56 (PSAP; *n*=2) and 1:1.32 (PKC-δ; *n*=2). Values are based on relative integrated *Volume* value (intensity × mm^2) normalized to LAMP-1 *Volume* value, and represent the means of independent experiments (*n*) on distinct lysosome preparations.

To confirm the localization of candidate proteins, colocalization experiments were visualized by fluorescent confocal microscopy with LAMP-1 as lysosome biomarker. As shown in Fig. 4 (lower panels), all candidate proteins colocalize to lysosomes with *RCA* values of 15.5% ±3.0 (*n*=6) and 26.2%±5.8 (*n*=6) for NSDHL: LAMP-1, 19.3%±0.9 (*n*=4) and 30.8%±2.6 (*n*=4) for PSAP:LAMP-1, and 23.2%±2.8 (*n*=6) and 33.7%±2.7 (*n*=6) for PKC-δ:LAMP-1, in control and CPT-treated cells, respectively. The annotated-spectra and iTRAQ reporter peaks for peptides of validated proteins presented in Fig. 4 are provided in Supplemental Table 4.

4. Discussion

Proteomics methods have been recently deployed to identify lysosome proteins (reviewed in [47]). The major aim of our study was to identify candidate proteins that accumulate at lysosomes, with a restrictive and limiting criteria consisting of very early phase of apoptosis when approximately less than 10% of the lysosome population presents partial membrane disruption or labilization in cells induced to undergo apoptosis by CPT, a DNA topoisomerase I inhibitor. By utilizing subcellular fractionation, iTRAQ reagent labeling, 1-D/IEF and LC-ESI-MS/MS-based technology for protein quantitation and identification, we were able to identify candidate proteins which are differentially expressed in lysosomes obtained from human cells triggered to undergo apoptosis. Recently, Yu et al. have reported subcellular proteome analysis of camptothecin analogue-treated NB4 cells, focusing on nuclear, ER, mitochondria and cytosolic proteins [48]. To the best of our knowledge, this is the first study describing the lysosome proteome at very early phase of CPT-induced apoptosis.

Only a few proteins have been shown to accumulate in lysosomes where they contribute to lysosome rupture or labilization during apoptosis, including phospholipase A2 and C, and LAPF [33–37]. These proteins were not detected in our study. This discrepancy could be due to the subcellular fractionation protocol used in these experiments, and to variations in biological responses, depending on the stimuli that provoke lysosomal labilization. Indeed, organelle purification and fractionation are challenging, particularly for membrane-bound small organelles like lysosome-related organelles, where communication with each other and remodeling occur frequently by complex membrane dynamics and transmembrane protein trafficking [45,49]. In addition to the dynamic nature of the organelles themselves, membrane-bound cellular organelles could often share comparable densities, which render purification to complete homogeneity by density gradient centrifugation untenable, if not impossible. Nevertheless, sequential density gradient centrifugation represents the best current technology and leads to high enrichment of organelles [45,49]. Because of these intrinsic limitations in membrane-bound organelle purification, in addition to validating protein candidate expression by Western blotting, protein candidate localization was also visualized by high-resolution fluorescence confocal microscopy. Keeping in mind the

dynamic nature of these organelles, and the restrictive and limiting criteria of the study consisting of experiments performed at very early phase of apoptosis when approximately less than 10% of the lysosome population presents partial membrane disruption or labilization, the expression and localization of representative protein candidates, initially identified in 1 experiment only, were also considered.

With these various approaches, 3 representative candidate proteins were validated, including NSDHL, PSAP and PKC-δ. NSDHL is a catalytic enzyme involved in cholesterol biosynthesis, removing 2 C-4 methyl groups in post-squalene cholesterol biosynthesis [50]. In turn, cholesterol, an essential component of biomembranes, is a major determinant of membrane fluidity. Membranes enriched in cholesterol with glycosphingolipids, sphingolipids and phospholipids can lead to the formation of lipid rafts and non-raft shell lipids with protein microdomain formation [51]. Interestingly, cholesterol content is know to be key determinant during endocytosis where lysosomal membranes are formed and prepared for digestion by a controlled lipid-sorting process [52]. Cholesterol accumulation to lysosomes has been associated with lysosomal dysfunctions in Niemann–Pick type C disease provoking autophagic stress and increased cell death [53–56], and cholesterol oxidation products have been reported to cause lysosomal destabilization and apoptosis [57]. Similarly, treatment of cells with inhibitors that block cholesterol transport out of the lysosome, including the amphiphile 3-beta-(2-(diethylamino)ethoxy)androst-5-en-17-one (U18666A), has been reported to provoke apoptosis [58,59], although cholesterol accumulation in mitochondrial membranes leads to inefficient Bax oligomerization [60]. Thus, molecular interplay between cholesterol segregation and partitioning, and cholesterol-dependent protein microdomain formation appear to contribute to many cellular functions, including lysosome-endocytosis, lysosome-autophagy and lysosome-apoptosis regulation. Further investigations to understand the role of NSDHL in cholesterol-mediated effect during early phase of lysosomal disruption during apoptosis will be challenging for the near future.

PKC-δ has been demonstrated to regulate apoptosis in response to various stimuli, including DNA-damaging agents [61–63]. The apoptotic function of PKC-δ has been associated with its localization and with the activation of multiple signaling proteins, including JNK, p38, ATM, AKT, cAbl, p73, DNA-PK, lamin, scramblase and, more recently, acid sphingomyelinase [64–66]. Interestingly, upon phorbol 12-myristate 13-acetate treament, PKC-δ has been shown to rapidly translocate to lysosomes where it phosphorylates and activates lysosomal acid sphingomyelinase, a key enzyme that catalyzes the degradation of membrane-bound sphingomyelin into phosphorylcholine and ceramide [66,67]. Formed of a single peptidic chain, PKC-δ contains an inhibitory pseudosubstrate domain that occludes the substrate-binding pocket, two membrane-binding domains (termed C1 and C2) and a conserved catalytic domain. The C1 domain forms a hydrophobic globular structure and coordinates with two Zn^{2+} ions to allow diaglycerol and phorbol ester binding and insertion inside apolar milieu of membranes [68,69]. The C2 domain comprise a characteristic 8-stranded antiparallel β-sandwich that also binds phospholipids but unlike other PKC isoforms, the C2 domain of PKC-δ does not required presence of Ca^{2+} ions. Upon its activation, PKC-δ autoinhibitory domain moves to open the phorbol ester-binding pocket and allows interaction of C1 and C2 domains with membrane lipids, resulting in its

translocation from the cytosol to sub-cellular membranes, including lysosomal membrane [66,67,70]. In this study, the observed increase in PKC-δ relocalization at lysosomes after CPT treatment strongly suggests that activation of acid sphingomyelinase, in turn, could raise ceramide levels, an event often associated with apoptosis induction [71]. DNA damaging agents including etoposide and NSC606985, a CPT analog, have been reported to induce a caspase-dependent proteolytic activation of PKC-δ into a 41 kDa catalytic fragment that activates the kinase [72–74]. In this study, with analysis performed at very early phase of apoptosis, the translocation of PKC-δ to lysosomes was not associated with its proteolytic cleavage, consistent with a previous study that has reported that PKC-δ cleavage occurred 24 h after NSC606985 treatment in U-937 cells [74].

Similarly, PSAP, the other candidate protein validated in this study, is the precursor of 4 lysosomal sphingolipid activator proteins (saposin A–D), that also play key roles in acid sphingomyelinase activation [75,76], and lysosomal membrane digestion during endocytosis [52]. PSAP and the saposins are membrane-pertubating and lipid-binding proteins that are essential for glycosphingolipid degradation of lysosomal membranes [52]. Recruited together at lysosomes after CPT treatment, NSDHL, PKC-δ and PSAP could possibly have drastic effects, leading to membrane fluidity, rapid ceramide accumulation, major changes in sphingolipid content, with glycosphingolipid degradation and lysosomal membrane disruption.

Several proteins associated with ER stress have also been identified by the proteomic approach. In U937 cells, we also noticed that CPT triggered typical morphological rearrangements of cells undergoing ER stress, with cells showing ER undergoing clumping and forming aggregates and/or small vesicles, 3 h post-CPT treatment [77,78] (data not shown). However, the connection between ER stress, appearance of aggregates and/or small vesicles and lysosome impairment has not been well documented. Given the importance of autophagy during organelle damage and stress, and the relation between autophagy and apoptosis, it will be of interest to pursue future studies in that direction.

In conclusion, iTRAQ reagent labeling with 1-D/IEF and LC-ESI-MS/MS approaches combined with the validation of expression/localization of candidate proteins, have permitted the identification of novel proteins that accumulate in lysosomes in the early phase of CPT-induced lysosome labilization and apoptosis. The exact consequences of accumulating these proteins in lysosomes for lysosome labilization and apoptosis are, yet, unknown. All of our 3 validated candidate proteins are related to biomembrane fluidity and dynamics, particularly cholesterol, sphingolipid and glycosphingolipid metabolism. Further functional studies are underway to investigate their importance for lysosome dysfunction and labilization during CPT-induced apoptosis.

Supplementary Material

Refer to Web version on PubMed Central for supplementary material.

Acknowledgments

This work was supported by a grant from the Canadian Institutes of Health Research to R.B. G.G.P. is a recipient of a Canadian Research Chair in Proteomics. N.P. obtained studentships from the Faculté des études supérieures (Université de Montréal) and from the Institut du cancer de Montréal and Canderel Inc. (Montréal, QC). CP received fellowship from Fonds de la recherche en santé du Québec (FRSQ). The authors thank Mr. Ovid Da Silva (Research Support Office, Research Centre, CHUM) for editing this manuscript.

Abbreviations

Ac-DEVD-AMC	acetyl-Asp-Glu-Val-Asp-7-amino-4-methylcoumarin
AO	acridine orange
BH	Bcl-2 homology
CPT	20-S-camptothecin lactone
EF	error factor
ER	endoplasmic reticulum
FC	fold change
iTRAQ	isobaric tag for relative and absolute quantitation
Ig	immunoglobulin
JC-1	5,5′,6,6′-tetrachloro-1,1′,3,3′-tetraethylbenzimidazolyl-carbocyanide iodide
MMTS	methyl-methane-thiosulfonate
NSDHL	sterol-4-alpha-carboxylate 3-dehydrogenase
PI	propidium iodide
PKC-δ	protein kinase C delta
PSAP	prosaposin
RCA	relative colocalization area
SD	standard deviation
SE	standard error
Z-RR-AMC	benzyloxycarbonyl-Arg-Arg-7-amino-4-methylcoumarin
1-D/IEF	one-dimensional isoelectric focusing
↓ΔΨm	loss of mitochondrial transmembrane potential

References

1. Brunk UT, Neuzil J, Eaton JW. Lysosomal involvement in apoptosis. Redox Rep. 2001; 6:91–7. [PubMed: 11450988]

2. Turk B, Stoka V, Rozman-Pungercar J, Cirman T, Droga-Mazovec G, Oreic K, et al. Apoptotic pathways: involvement of lysosomal proteases. Biol Chem. 2002; 383:1035–44. [PubMed: 12437086]

3. Guicciardi ME, Leist M, Gores GJ. Lysosomes in cell death. Oncogene. 2004; 23:2881–90. [PubMed: 15077151]

4. Terman A, Kurz T, Gustafsson B, Brunk UT. Lysosomal labilization. IUBMB Life. 2006; 58:531–9. [PubMed: 17002981]

5. Brunk UT, Svensson I. Oxidative stress, growth factor starvation and Fas activation may all cause apoptosis through lysosoma leak. Redox Rep. 1999; 4:3–11. [PubMed: 10714269]

6. Brunk UT, Dalen H, Roberg K, Hellquist HB. Photo-oxidative disruption of lysosomal membranes causes apoptosis of cultured human fibroblasts. Free Radic Biol Med. 1997; 23:616–26. [PubMed: 9215807]

7. Boya P, Andreau K, Poncet D, Zamzami N, Perfettini JL, Metivier D, et al. Lysosomal membrane permeabilization induces cell death in a mitochondrion-dependent fashion. J Exp Med. 2003; 197:1323–34. [PubMed: 12756268]

8. Guicciardi ME, Deussing J, Miyoshi H, Bronk SF, Svingen PA, Peters C, et al. Cathepsin B contributes to TNF-alpha-mediated hepatocyte apoptosis by promoting mitochondrial release of cytochrome c. J Clin Invest. 2000; 106:1127–37. [PubMed: 11067865]

9. Kagedal K, Zhao M, Svensson I, Brunk UT. Sphingosine-induced apoptosis is dependent on lysosomal proteases. Biochem J. 2001; 359:335–43. [PubMed: 11583579]

10. Heinrich M, Wickel M, Schneider-Brachert W, Sandberg C, Gahr J, Schwandner R, et al. Cathepsin D targeted by acid sphingomyelinase-derived ceramide. EMBO J. 1999; 18:5252–63. [PubMed: 10508159]

11. Hishita T, Tada-Oikawa T, Tohyama K, Miura Y, Nishihara T, Tohyama Y, et al. Caspase-3 activation by lysosomal enzymes in cytochrome c-independent apoptosis in myelodysplastic syndrome-derived cell line P39. Cancer Res. 2001; 61:2878–84. [PubMed: 11306462]

12. Paquet C, Beauchemin M, Bertrand R. Caspase- and mitochondrial dysfunction-dependent mechanisms of lysosomal leakage and cathepsin B activation in DNA damage-induced apoptosis. Leukemia. 2005; 19:784–91. [PubMed: 15759029]

13. Broker LE, Huisman C, Span SW, Rodriguez JA, Kruyt FA, Giaccone G. Cathepsin B mediates caspase-independent cell death induced by microtubule stabilizing agents in non-small cell lung cancer cells. Cancer Res. 2004; 64:27–30. [PubMed: 14729603]

14. Kluck RM, Martin SJ, Hoffman BM, Zhou JS, Green DR, Newmeyer DD. Cytochrome C activation of Cpp32-like proteolysis plays a critical role in a Xenopus cell-free apoptosis system. EMBO J. 1997; 16:4639–49. [PubMed: 9303308]

15. Marzo I, Brenner C, Zamzami N, Jurgensmeier JM, Susin SA, Vieira HLA, et al. Bax and adenine nucleotide translocator cooperate in the mitochondrial control of apoptosis. Science. 1998; 281:2027–31. [PubMed: 9748162]

16. Matsuyama S, Xu QL, Velours J, Reed JC. The mitochondrial F0F1-ATPase proton pump is required for function of the proapoptotic protein Bax in yeast and mammalian cells. Mol Cell. 1998; 1:327–36. [PubMed: 9660917]

17. Shimizu S, Narita M, Tsujimoto Y. Bcl-2 family proteins regulate the release of apoptogenic cytochrome c by the mitochondrial channel VDAC. Nature. 1999; 399:483–7. [PubMed: 10365962]

18. Vander Heiden MG, Chandel NS, Williamson EK, Schumacker PT, Thompson CB. Bcl-X(L) regulates the membrane potential and volume homeostasis of mitochondria. Cell. 1997; 91:627–37. [PubMed: 9393856]

19. Vander Heiden MG, Thompson CB. Bcl-2 proteins: regulators of apoptosis or of mitochondrial homeostasis? Nat Cell Biol. 1999; 1:E209–16. [PubMed: 10587660]

20. Kroemer G, Galluzzi L, Brenner C. Mitochondrial membrane permeabilization in cell death. Physiol Rev. 2007; 87:99–163. [PubMed: 17237344]

21. Reed JC. Proapoptotic multidomain Bcl-2/Bax-family proteins: mechanisms, physiological roles, andtherapeutic opportunities. Cell Death Differ. 2006; 13:1378–86. [PubMed: 16729025]

22. Adams JM, Cory S. The Bcl-2 apoptotic switch in cancer development and therapy. Oncogene. 2007; 26:1324–37. [PubMed: 17322918]
23. Chittenden T, Flemington C, Houghton AB, Ebb RG, Gallo GJ, Elangovan B, et al. A conserved domain in Bak, distinct from BH1 and BH2, mediates cell death and protein binding functions. EMBO J. 1995; 14:5589–96. [PubMed: 8521816]
24. Polster BM, Kinnally KW, Fiskum G. BH3 death domain peptide induces cell type-selective mitochondrial outer membrane permeability. J Biol Chem. 2001; 276:37887–94. [PubMed: 11483608]
25. Chittenden T. BH3 domains: intracellular death-ligands critical for initiating apoptosis. Cancer Cell. 2002; 2:165–6. [PubMed: 12242145]
26. Kuwana T, Bouchier-Hayes L, Chipuk JE, Bonzon C, Sullivan BA, Green DR, et al. BH3 domains of BH3-only proteins differentially regulate Bax-mediated mitochondrial membrane permeabilization both directly and indirectly. Mol Cell. 2005; 17:525–35. [PubMed: 15721256]
27. Kim H, Rafiuddin-Shah M, Tu HC, Jeffers JR, Zambetti GP, Hsieh JJ, et al. Hierarchical regulation of mitochondrion-dependent apoptosis by Bcl-2 subfamilies. Nat Cell Biol. 2006; 8:1348–58. [PubMed: 17115033]
28. Chen L, Willis SN, Wei A, Smith BJ, Fletcher JI, Hinds MG, et al. Differential targeting of prosurvival Bcl-2 proteins by their BH3-only ligands allows complementary apoptotic function. Mol Cell. 2005; 17:393–403. [PubMed: 15694340]
29. Willis SN, Chen L, Dewson G, Wei A, Naik E, Fletcher JI, et al. Proapoptotic Bak is sequestered by Mcl-1 and Bcl-xL, but not Bcl-2, until displaced by BH3-only proteins. Genes Dev. 2005; 19:1294–305. [PubMed: 15901672]
30. Willis SN, Fletcher JI, Kaufmann T, van Delft MF, Chen L, Czabotar PE, et al. Apoptosis initiated when BH3 ligands engage multiple Bcl-2 homologs, not Bax or Bak. Science. 2007; 315:856–9. [PubMed: 17289999]
31. Hu JS, Li YB, Wang JW, Sun L, Zhang GJ. Mechanism of lysophosphatidylcholine-induced lysosome destabilization. J Membr Biol. 2007; 215:27–35. [PubMed: 17510762]
32. Zhao M, Brunk UT, Eaton JW. Delayed oxidant-induced cell death involves activation of phospholipase A2. FEBS Lett. 2001; 509:399–404. [PubMed: 11749963]
33. Hiraoka M, Abe A, Lu Y, Yang K, Han X, Gross RW, et al. Lysosomal phospholipase A2 and phospholipidosis. Mol Cell Biol. 2006; 26:6139–48. [PubMed: 16880524]
34. Wang X, Wang LL, Zhang GJ. Guanosine 5′-[gamma-thio] triphosphate-mediated activation of cytosol phospholipase C caused lysosomal destabilization. J Membr Biol. 2006; 211:55–63. [PubMed: 16988860]
35. Wang X, Zhao HF, Zhang GJ. Mechanism of cytosol phospholipase C and sphingomyelinase-induced lysosome destabilization. Biochimie. 2006; 88:913–22. [PubMed: 16580116]
36. Zhao HF, Wang X, Zhang GJ. Lysosome destabilization by cytosolic extracts, putative involvement of Ca(2+)/phospholipase C. FEBS Lett. 2005; 579:1551–6. [PubMed: 15733872]
37. Chen W, Li N, Chen T, Han Y, Li C, Wang Y, et al. The lysosome-associated apoptosis-inducing protein containing the pleckstrin homology (PH) and FYVE domains (LAPF), representative of a novel family of PH and FYVE domain-containing proteins, induces caspase-independent apoptosis via the lysosomal-mitochondrial pathway. J Biol Chem. 2005; 280:40985–95. [PubMed: 16188880]
38. Salvioli S, Ardizzoni A, Franceschi C, Cossarizza A. Jc-1, but not Dioc(6)(3) or rhodamine 123, is a reliable fluorescent probe to assess Delta–Psi changes in intact cells; Implications for studies on mitochondrial functionality during apoptosis. FEBS Lett. 1997; 411:77–82. [PubMed: 9247146]
39. Bertrand R, Sarang M, Jenkin J, Kerrigan D, Pommier Y. Differential induction of secondary DNA fragmentation by topoisomerase II inhibitors in human tumor cell lines with amplified c-myc expression. Cancer Res. 1991; 51:6280–5. [PubMed: 1933888]
40. Storrie B, Madden EA. Isolation of subcellular organelles. Methods Enzymol. 1990; 182:203–25. [PubMed: 2156127]
41. Paquet C, Schmitt E, Beauchemin M, Bertrand R. Activation of multidomain and BH3-only pro-apoptotic Bcl-2 family members in p53-defective cells. Apoptosis. 2004; 9:815–31. [PubMed: 15505424]

42. Shilov IV, Seymour SL, Patel AA, Loboda A, Tang WH, Keating SP, et al. The Paragon Algorithm, a next generation search engine that uses sequence temperature values and feature probabilities to identify peptides from tandem mass spectra. Mol Cell Proteomics. 2007; 6:1638–55. [PubMed: 17533153]
43. Schmitt E, Cimoli G, Steyaert A, Bertrand R. Bcl-xL modulates apoptosis induced by anticancer drugs and delays DEVDase and DNA fragmentation-promoting activities. Exp Cell Res. 1998; 240:107–21. [PubMed: 9570926]
44. Sané AT, Bertrand R. Distinct steps in DNA fragmentation pathway during camptothecin-induced apoptosis involved caspase-, benzyloxycarbonyl- and N-tosyl-L-phenylalanylchloromethyl ketone-sensitive activities. Cancer Res. 1998; 58:3066–72. [PubMed: 9679972]
45. Hu ZZ, Valencia JC, Huang H, Chi A, Shabanowitz J, Hearing VJ, et al. Comparative bioinformatics analyses and profiling of lysosome-related organelle proteomes. Int J Mass Spectrom. 2007; 259:147–60. [PubMed: 17375895]
46. Casey TM, Meade JL, Hewitt EW. Organelle proteomics: identification of the exocytic machinery associated with the natural killer cell secretory lysosome. Mol Cell Proteomics. 2007; 6:767–80. [PubMed: 17272266]
47. Callahan JW, Bagshaw RD, Mahuran DJ. The integral membrane of lysosomes: its proteins and their roles in disease. J Proteomics. 2009; 72:23–33. [PubMed: 19068244]
48. Yu Y, Wang LS, Shen SM, Xia L, Zhang L, Zhu YS, et al. Subcellular proteome analysis of camptothecin analogue NSC606985-treated acute myeloid leukemic cells. J Proteome Res. 2007; 6:3808–18. [PubMed: 17655343]
49. Takamori S, Holt M, Stenius K, Lemke EA, Gronborg M, Riedel D, et al. Molecular anatomy of a trafficking organelle. Cell. 2006; 127:831–46. [PubMed: 17110340]
50. Caldas H, Herman GE. NSDHL, an enzyme involved in cholesterol biosynthesis, traffics through the Golgi and accumulates on ER membranes and on the surface of lipid droplets. Hum Mol Genet. 2003; 12:2981–91. [PubMed: 14506130]
51. Haucke V, DiPaolo G. Lipids and lipid modifications in the regulation of membrane traffic. Curr Opin Cell Biol. 2007; 19:426–35. [PubMed: 17651957]
52. Kolter T, Sandhoff K. Principles of lysosomal membrane digestion: stimulation of sphingolipid degradation by sphingolipid activator proteins and anionic lysosomal lipids. Annu Rev Cell Dev Biol. 2005; 21:81–103. [PubMed: 16212488]
53. Beltroy EP, Liu B, Dietschy JM, Turley SD. Lysosomal unesterified cholesterol content correlates with liver cell death in murine Niemann–Pick type C disease. J Lipid Res. 2007; 48:869–81. [PubMed: 17220530]
54. Bi X, Liao G. Autophagic-lysosomal dysfunction and neurodegeneration in Niemann–Pick Type C mice: lipid starvation or indigestion? Autophagy. 2007; 3:646–8. [PubMed: 17921694]
55. Liao G, Yao Y, Liu J, Yu Z, Cheung S, Xie A, et al. Cholesterol accumulation is associated with lysosomal dysfunction and autophagic stress in Npc1 −/− mouse brain. Am J Pathol. 2007; 171:962–75. [PubMed: 17631520]
56. Pacheco CD, Lieberman AP. Lipid trafficking defects increase Beclin-1 and activate autophagy in Niemann–Pick type C disease. Autophagy. 2007; 3:487–9. [PubMed: 17611388]
57. Yuan XM, Li W, Brunk UT, Dalen H, Chang YH, Sevanian A. Lysosomal destabilization during macrophage damage induced by cholesterol oxidation products. Free Radic Biol Med. 2000; 28:208–18. [PubMed: 11281288]
58. Koh CH, Cheung NS. Cellular mechanism of U18666A-mediated apoptosis in cultured murine cortical neurons: bridging Niemann–Pick disease type C and Alzheimer's disease. Cell Signal. 2006; 18:1844–53. [PubMed: 16797161]
59. Koh CH, Qi RZ, Qu D, Melendez A, Manikandan J, Bay BH, et al. U18666A-mediated apoptosis in cultured murine cortical neurons: role of caspases, calpains and kinases. Cell Signal. 2006; 18:1572–83. [PubMed: 16446076]
60. Lucken-Ardjomande S, Montessuit S, Martinou JC. Bax activation and stress-induced apoptosis delayed by the accumulation of cholesterol in mitochondrial membranes. Cell Death Differ. 2008; 15:484–93. [PubMed: 18084240]

61. Brodie C, Blumberg PM. Regulation of cell apoptosis by protein kinase C delta. Apoptosis. 2003; 8:19–27. [PubMed: 12510148]
62. Basu A. Involvement of protein kinase C delta in DNA damage-induced apoptosis. J Cell Mol Med. 2003; 7:341–50. [PubMed: 14754503]
63. Blass M, Kronfeld I, Kazimirsky G, Blumberg PM, Brodie C. Tyrosine phosphorylation of protein kinase C delta is essential for its apoptotic effect in response to etoposide. Mol Cell Biol. 2002; 22:182–95. [PubMed: 11739733]
64. Yoshida K. PKC delta signaling: mechanisms of DNA damage response and apoptosis. Cell Signal. 2007; 9:892–901.
65. Gomel R, Xiang C, Finniss S, Lee HK, Lu W, Okhrimenko H, et al. The localization of protein kinase C delta in different subcellular sites affects its proapoptotic and antiapoptotic functions and the activation of distinct downstream signaling pathways. Mol Cancer Res. 2007; 5:627–39. [PubMed: 17579121]
66. Zeidan YH, Hannun YA. Activation of acid sphingomyelinase by protein kinase C delta-mediated phosphorylation. J Biol Chem. 2007; 282:11549–61. [PubMed: 17303575]
67. Zeidan YH, Wu BX, Jenkins RW, Obeid LM, Hannun YA. A novel role for protein kinase C delta-mediated phosphorylation of acid sphingomyelinase in UV light-induced mitochondrial injury. FASEB J. 2008; 22:183–93. [PubMed: 17698617]
68. Chow W. Membrane targeting by C1 and C2 domains. J Biol Chem. 2001; 276:32407–10. [PubMed: 11432875]
69. Zhang G, Kazanietz MG, Blumberg PM, Hurley JH. Crystal structure of the Cys2 activator-binding domain of protein kinase Cδ in complex with phorbol esters. Cell. 1995; 81:917–24. [PubMed: 7781068]
70. Wang QJ, Bhattacharyya D, Garfield S, Nacro K, Marquez VE, Blumberg PM. Differential localization of protein kinase C delta by phorbol esters and related compounds using a fusion protein with green fluorescent protein. J Biol Chem. 1999; 274:37233–9. [PubMed: 10601287]
71. Siskind LJ. Mitochondrial ceramide and the induction of apoptosis. J Bioenerg Biomembr. 2005; 37:143–53. [PubMed: 16167171]
72. Khwaja A, Tatton L. Caspase-mediated proteolysis and activation of protein kinase Cdelta plays a central role in neutrophil apoptosis. Blood. 1999; 94:291–301. [PubMed: 10381525]
73. Shin SY, Kim CG, Ko J, Min DS, Chang JS, Ohba M, et al. Transcriptional and post-transcriptional regulation of the PKC delta gene by etoposide in L1210 murine leukemia cells: implication of PKC delta autoregulation. J Mol Biol. 2004; 340:681–93. [PubMed: 15223313]
74. Song MG, Gao SM, Du KM, Xu M, Yu Y, Zhou YH, et al. Nanomolar concentration of NSC606985, a camptothecin analog, induces leukemic-cell apoptosis through protein kinase Cdelta-dependent mechanisms. Blood. 2005; 105:3714–21. [PubMed: 15671440]
75. Linke T, Wilkening G, Lansmann S, Moczall H, Bartelsen O, Weisgerber J, et al. Stimulation of acid sphingomyelinase activity by lysosomal lipids and sphingolipid activator proteins. Biol Chem. 2001; 382:283–90. [PubMed: 11308026]
76. Ferlinz K, Linke T, Bartelsen O, Weiler M, Sandhoff K. Stimulation of lysosomal sphingomyelin degradation by sphingolipid activator proteins. Chem Phys Lipids. 1999; 102:35–43. [PubMed: 11001559]
77. Terrinoni A, Ranalli M, Cadot B, Leta A, Bagetta G, Vousden KH, et al. p73-alpha is capable of inducing scotin and ER stress. Oncogene. 2004; 23:3721–5. [PubMed: 15116103]
78. Moenner M, Pluquet O, Bouchecareilh M, Chevet E. Integrated endoplasmic reticulum stress responses in cancer. Cancer Res. 2007; 67:10631–4. [PubMed: 18006802]

Appendix A. Supplementary data

Supplementary data associated with this article can be found, in the online version, at doi: 10.1016/j.jprot.2009.04.003.

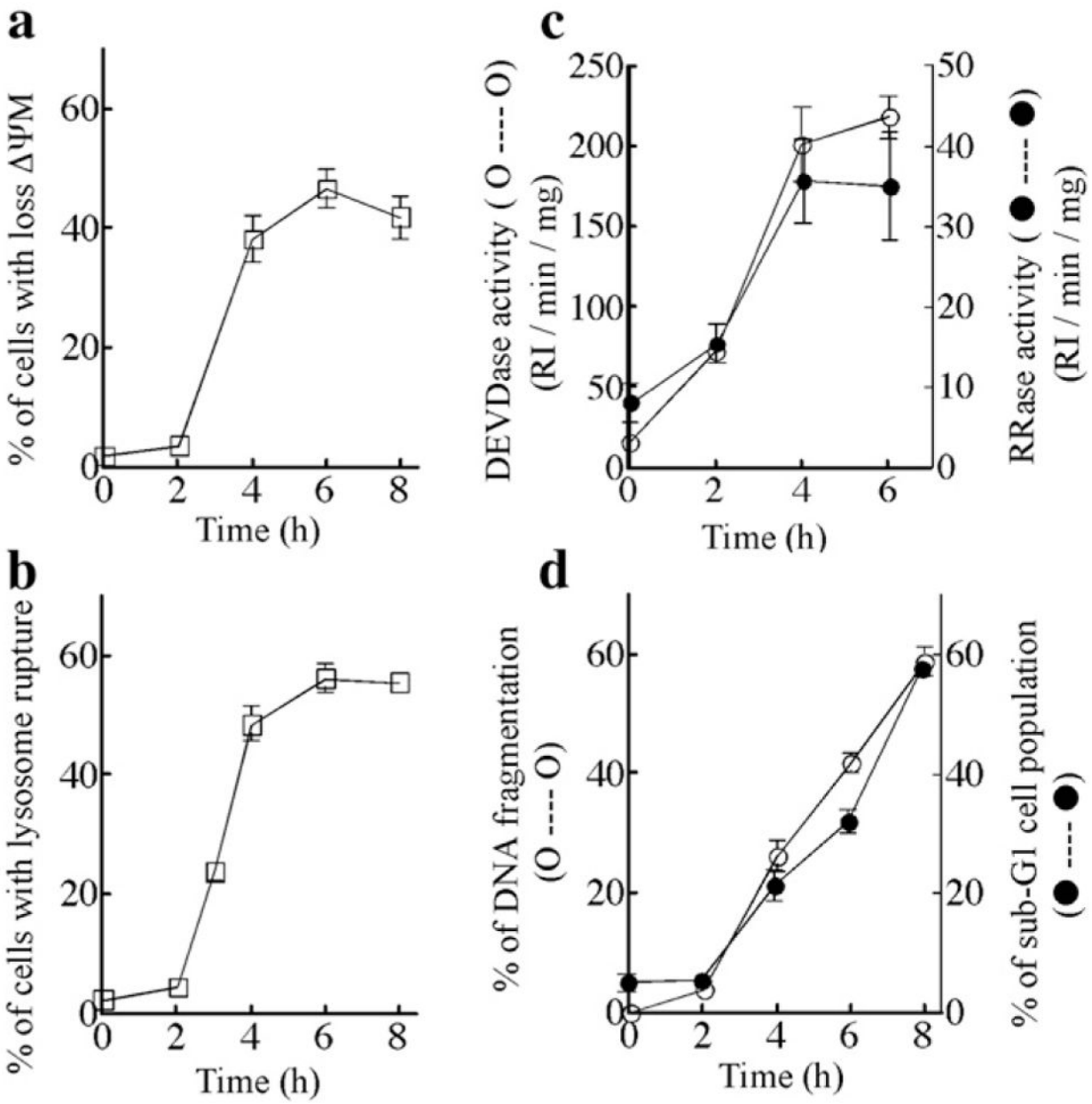

Fig. 1.

Parameters of CPT-induced apoptosis in U-937 cells. U-937 cells were treated with 1.0 μM CPT for 30 min. At the indicated times (h) after CPT treatment, a) the percentage of total cells with ↓ΔΨm, b) the percentage of total cells with lysosome rupture or labilization, c) the kinetics of caspase-3-like (open circles) and cathepsin B (closed circles) activities, and d) the percentage of DNA fragmentation (open circles) and sub-G_1 death cells (closed circles) were quantified as described in Experimental Procedures. Symbols represent the means±SE of at least 4 independent experiments.

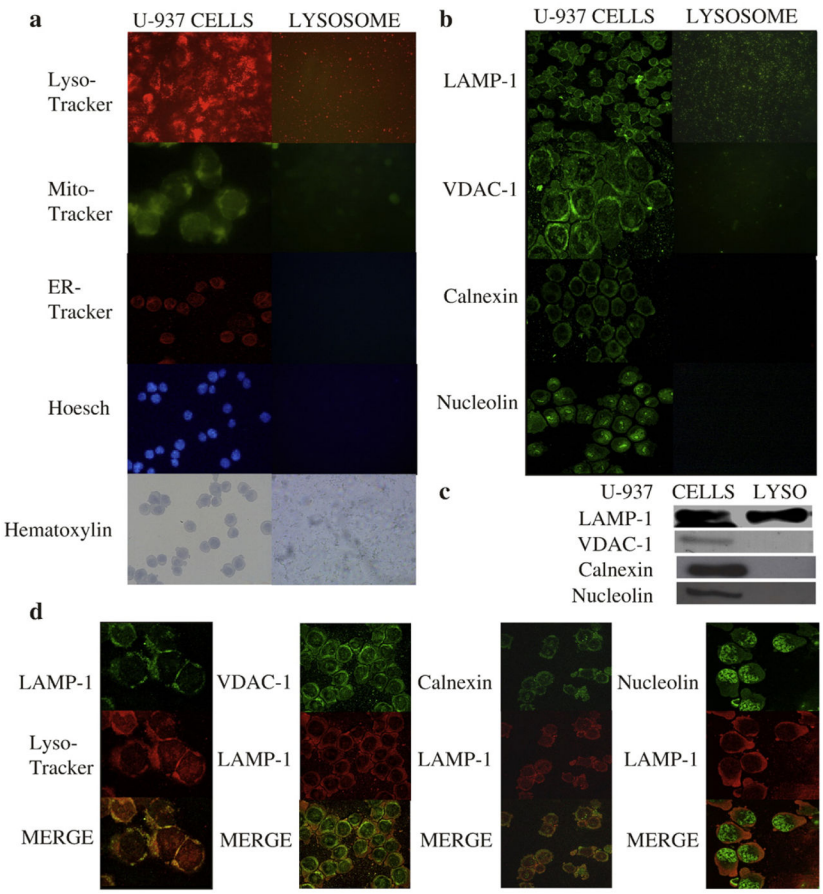

Fig. 2.

Purity of enriched lysosome preparations obtained by 2-step sequential density gradients. Lysosomes from U-937 cells were purified by 2-step sequential density gradients and a) U-937 cells and enriched lysosome preparations were stained *in situ* with the fluorescent biomarkers LysoTracker RED/DND-99 (lysosome), MitoTracker Green/FM (mitochondria), ER-Tracker Red dye (endoplasmic reticulum, ER) and Hoechst 33342 (nucleus), and observed under a fluorescent microscope. Hematoxylin staining is also shown; b) Cells and enriched lysosome preparations were labeled with specific antibodies directed against the protein biomarkers LAMP-1 (lysosome), VDAC-1 (mitochondria), Calnexin (ER) and Nucleolin (nucleus) and monitored by fluorescence microscopy; c) Protein aliquots of enriched lysosome preparations were run on SDS-PAGE for Western blotting using anti-LAMP-1 (lysosome biomarker), anti-VDAC-1 (mitochondria biomarker), anti-Calnexin (ER biomarker) and anti-Nucleolin (nuclear biomarker) to monitor the purity of the lysosome preparations; d) Colocalization of LAMP-1 with the fluorescent biomarker LysoTracker RED/DND-99. Note that VDAC-1:LAMP-1, Calnexin:LAMP-1 and Nucleolin:LAMP-1 do not significantly colocalized together. All representative of 3 or 4 independent experiments.

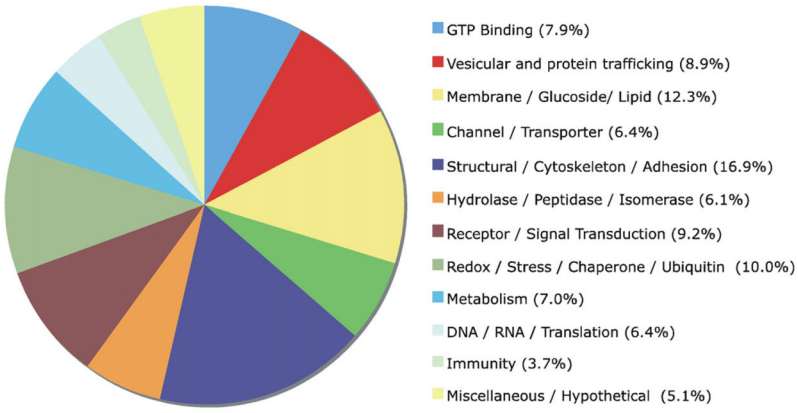

Fig. 3.

Functional classification of the proteins identified in 1 reference experiment. All data associated with this graph are presented in Supplemental Table 1. Only proteins including at least 2 peptides above 80% confidence were considered.

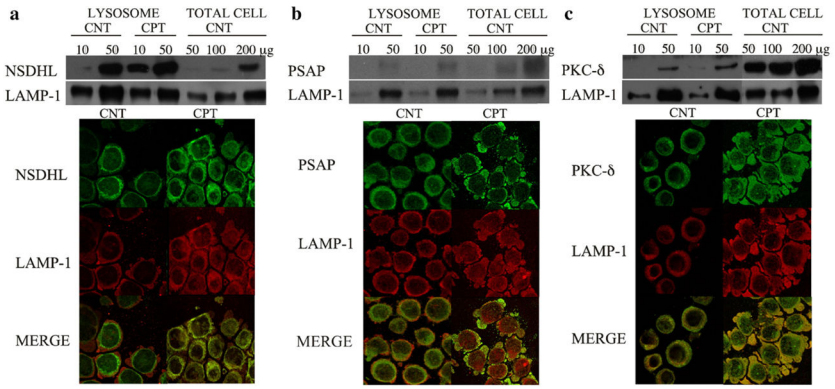

Fig. 4.

Validation of differentially-expressed representative protein candidates. To validate the expression/localization of representative candidate proteins, in the upper panels, protein aliquots (10 and 50 µg) of enriched lysosome preparations obtained from control (*C*) and CPT-treated cells (3 h post-treatment; CPT) were run on SDS-PAGE for Western blotting using specific antibodies against NSDHL (a), PSAP (b) and PKC-δ (c). LAMP-1 serves as a loading control; protein extracts obtained from whole cells are antibody controls. Relative ratios after CPT treatment were determined by relative densitometry analysis of light radiographs normalized to LAMP-1 intensity levels. Data in the Results section represent the means of (*n*) independent experiments. Lower panels: colocalization of NSDHL (a), PSAP (b) and PKC-δ (c) (fluorescein-labeled) and LAMP-1 (Red Texas-labeled), in control (*C*) and CPT-treated cells (3 h post-treatment; CPT). Data in the Results section are expressed as *Relative Colocalization Area* (*RCA*) values, and represent the means±SD of (*n*) independent experiments.

Table 1

Candidate proteins differentially expressed in enriched lysosome preparations from early apoptotic U-937 cells.

A	Accession number	Name and *synonym*	Experiment 1						Experiment 2					
			***Unique* peptide (*total* count)**	**% Cov**	**Ratio**	**±S.D. or (±range)**	***P*-value**	**EF**	***Unique* peptide (*total* count)**	**% Cov**	**Ratio**	**±S.D. or (±range)**	***P*-value**	**EF**
	Level 1													
	UP10000456547/ UPI000047EFF7/ Q15005	Signal peptidase complex subunit 2 (SPCS2); *Microsomal signal peptidase 25 kDa subunit*	3 (5)	3.98	1.7361	±1.4002	0.1184	2.1237	2 (5)	4.02	1.6131	±0.3741	0.0148	1.3816
	P14174	Macrophage migration inhibitory factor (MIF); *Glycosylation inhibiting factor*	1 (8)*	7.83	1.6405	±0.0927	4.162E-10	1.0403	1 (16)*	7.83	1.4427	±0.1522	1.850E-11	1.0483
	Level 2													
	P16949/ A2A2D2	Stathmin 1/oncoprotein 18; *Leukemia-associated phosphoprotein p18*	1 (3)*	6.90	2.5295	±0.3662	0.0078	1.4258	6 (18)	34.23	1.0283	±0.2202	0.4639	1.0804
	Q15738	NAD(P) dependent steroid dehydrogenase-like (NSDHL); *Sterol-4-alpha-carboxylate 3-dehydrogenase, decarboxylating*	1 (1)*	2.39	1.9351	N.A.	0.302209	7.862	4 (6)	16.09	1.0944	±0.5346	0.5894	1.4731
	P63000/ A4D2P0	Ras-related C3 botulinum toxin substrate 1	2 (7)	9.95	1.6060	±0.1425	8.814E–08	1.0719	3 (7)	17.18	1.1230	±0.1668	0.0004	1.0782
	UPI0000EFE353/ P60953	Cell Division Cycle 42 (CDC42); *G25K GTP-binding protein*	5 (10)	27.75	1.5720	±0.3572	6.150E-05	1.1653	5 (34)	31.41	1.0060	±0.1871	0.8993	1.1154
	Q06830	Peroxiredoxin-1 (PRDX1)	4 (14)	21.11	1.4477	±0.2136	1.127E-06	1.0985	5 (11)	25.13	1.1125	±0.0710	0.0075	1.0728
	P30040	Endoplasmic reticulum protein ERp29 precursor	3 (10)	12.26	1.0516	±0.3415	0.6662	1.2816	2 (5)	8.43	1.9656	±0.5804	0.0076	1.4580
	O95881	Thioredoxin domain-containing protein 12 precursor (TXD12); *Thioredoxin protein p19, ERP19*	1 (1)*	5.23	1.1338	N.A.	N.A.	N.A.	2 (4)	13.37	1.6015	±0.2738	0.0170	1.3650
	P07237	Protein disulfide-isomerase precursor (PDIA1); *procollagenproline, 2-oxoglutarate 4-dioxygenase, beta polypeptide*	8 (23)	13.39	1.1377	±0.1660	6.834E-05	1.0580	28 (230)	50.00	1.4980	±0.3184	0.0000	1.0325
	P13667	Protein disulfide-isomerase A4 precursor (PDIA4)	10 (30)	13.80	1.1750	±0.3721	0.0019	1.1028	7 (18)	9.61	1.4855	±0.3662	1.180E-06	1.1288
	P30101	Protein disulfide-isomerase A3 precursor (PDIA3)	14 (38)	18.61	1.0449	±0.2759	0.2092	1.0719	11 (61)	22.18	1.5080	±0.2409	1.031E-24	1.0530
	Level 3													
	Q5QNW6	Histone H2B type 2-F	8 (42)	34.92	2.8113	±0.5410	1.285E-04	1.1363	N.D.					

	Accession number	Name and *synonym*	Experiment 1						Experiment 2					
			Unique peptide (*total* count)	% Cov	Ratio	±S.D. or (±range)	*P*-value	EF	*Unique* peptide (*total* count)	% Cov	Ratio	±S.D. or (±range)	*P*-value	EF
A														
	Q5JQ37	Prosaposin (variant Gaucher disease and variant metachromatic leukodystrophy)	N.D.						4 (17)	4.29	1.6085	±0.1582	4.105E-09	1.0960
	UPI000054B38F/ A8K3K8	Carboxylesterase 1 isoform c precursor	N.D.						6 (15)	12.01	1.5551	±0.1927	1.228E-09	1.0742
	UPI000013D53C/	N(4)-(beta-N-acetylglucosaminyl)-L-asparaginase precursor; *Glycosylasparaginase beta c, Aspartylglucosaminidase*	N.D.						2 (7)	3.76	1.4754	±0.5509	0.0154	1.3397
	P20933 UPI00002263A8/ NM198901	Sorcin isoform b	N.D.						3 (6)	10.93	1.4086	±0.2776	0.0079	1.2389
	Q05655	Protein kinase C delta type	N.D.						3 (9)	5.77	1.2469	±0.2035	0.0026	1.1340
B														
	Level 1													
	Q10471	UDP-N-acetyl-alpha-D-galactosamine: polypeptide N-acetylgalactosaminyltransferase 2 (GalNAc-T2)	2 (4)	4.90	0.6784	±0.1195	0.0231	1.3320	2 (2)	3.33	0.6820	(±0.1356)	0.0176	1.3136
	Q92896	Golgi apparatus protein 1 precursor (GSLG1); *Cysteine-rich fibroblast growth factor receptor, E-selectin ligand 1*	6 (8)	3.31	0.5613	±0.0910	1.129E-06	1.1504	1 (1)*	0.84	0.7235	N.A.	0.2851	2.6198
	Level 2													
	Q92520	Protein FAM3C precursor	3 (5)	7.93	0.5597	±0.0946	0.0014	1.2345	2 (2)	11.45	0.9794	(±0.3107)	0.9585	56.6481
	Q9UIQ6	Leucyl/cystinyl aminopeptidase (LNPEP)	2 (4)	2.73	0.6625	±0.1899	0.0814	1.6598	1 (12)*	1.46	0.9762	±0.2302	0.8547	1.3205
	Level 3													
	Q13425	Beta-2-syntrophin; *Dystrophin-associated protein A1*	2 (3)	4.81	0.6275	±0.0464	0.0086	1.2059	N.D.					
	Q8TAF6	Acyl-CoA synthetase long-chain family member 4	2 (3)	2.69	0.6921	±0.0473	0.0021	1.1232	N.D.					
	Q14321/ Q9BXA0	High-mobility group box 1 (HMG-1)	4 (9)	13.49	0.6975	±0.0988	1.324E-05	1.1176	N.D.					
		C-X-C chemokine receptor type 4 (CXCR4); *CD184 antigen*	2 (2)	5.68	0.7067	(±0.0422)	0.0085	1.2545	N.D.					
	Q9BVA1	Tubulin beta-2B chain	N.D.						9 (93)	31.46	0.6916	±0.2504	0.022414	1.2733

A: Up-regulated; B: Down-regulated; N.D.: Not-detected; N.A.: Not-applicable.

Level 1: Differentially expressed in 2 experiments.

Level 2: Differentially expressed in 1 experiment and detected in 2 experiments.

Level 3: Differentially expressed in 1 experiment and detected in 1 experiment only.

Standard deviation±S.D. were calculated from ratio values at *n* count ≥3, and *range* (±range) at *n* count = 2 by MicrosoftExcel software (v 11.2.3).

For protein identification with *unique-peptide**, the annotated spectra are provided in Supplemental Table 3.

All peptides for identification and quantification of candidate proteins are listed in Supplemental Table 2.

iTRAQ protein ratios (m/z 117/114) were calculated by ProteinPilot software (v.2.0) based on the weighted average *Log ratios* of peptides; and *ratio values* were corrected for experimental bias using the median average protein *ratio* as the correction factor.

Significance of *iTRAQ protein ratios* is expressed as *p-value* calculated by ProteinPilot software (v.2.0).

Accuracy of i*TRAQ protein ratios* was assessed by the *error factors values* (EF), calculated by ProteinPilot software (v.2.0).